An Effective Pseudopotential for Modeling Gold Surface Slabs for Ab Initio Simulations

Roger Rousseau,*[a] Riccardo Mazzarello,[a, b, c] and Sandro Scandolo[b, c]

Dedicated to Professor Michele Parrinello on the occasion of his 60th birthday.

Self-assembled monolayers (SAMs) of sulfur-containing organic molecules on bulk gold surfaces are among some of the currently most-studied molecule/metal interfaces, with potential applications ranging from nanolithography[1] and molecular electronics[2] to biosensors.[3] As such, there has been an intense effort on the part of the atomistic-simulations community to model the structures, energetics and spectroscopic properties of these materials.[4–12] However, there is still much debate in the literature regarding the nature of the thiolate–metal interaction[13] as well as the nature of the adsorption sites of the thiols[14,15] and possible low-temperature superstructures.[16] With the notable exception of ref. [17], where ab initio molecular dynamics (AIMD) simulations have been performed to model the pulling of a single thiolate from a Au surface, there has been little attention paid to the role of finite-temperature effects in these materials by the ab initio electronic-structure community. This is despite the fact that gold is known to be a very dynamical element that exhibits exceptional diffusivity and mobility. Though it is possible to model the dynamical behavior of Au via effective interatomic potentials,[18] there currently is no *reliable* interatomic potential to model the molecule–metal interaction. In principle, AIMD would be a valuable tool to address these issues, but its applicability is severely limited by its computational cost, both in terms of the required large system sizes[7] and simulation times. Specifically, the modeling of a bulk Au surface requires slab models of 4–6 atomic layers in thickness[9] with each Au atom having a minimal number of $11\,e^-$. As a result even a simple calculation providing the equivalent surface area to adsorb only four thiolate molecules requires around 600–1000 valence electrons. The current article is aimed at addressing this issue by employing an effective $1\,e^-$ valence-electron pseudopotential to emulate the behavior of the bulk gold substrate. The idea follows from the consideration that d electrons

[a] *Prof. Dr. R. Rousseau, Dr. R. Mazzarello*
International School For Advanced Studies (ISAS/SISSA)
Via Beirut 4, 34014 Trieste (Italy)
Fax: (+39) 040-224-0354
E-mail: rroussea@ictp.trieste.it

[b] *Dr. R. Mazzarello, Prof. Dr. S. Scandolo*
The Abdus Salam International Center for Theoretical Physics (ICTP)
Strada Costiera 11, 34014 Trieste (Italy)

[c] *Dr. R. Mazzarello, Prof. Dr. S. Scandolo*
INFM/Democritos National Simulation Center
34014 Trieste (Italy)

  DOI: 10.1002/cphc.200400615

of the interfacial Au atoms are essential to describe bonding with the thiolate, while Au atoms further below the surface are essentially bulklike and their only role is to provide a matching for the delocalized s-like component of the interfacial wavefunctions. This construct places the focus of the computational effort on the thiolate molecules and Au atoms that are directly at the surface and thus allows for more efficient AIMD simulations of surface-slab models.

Methods

Our electronic-structure calculations are performed with the CPMD code,[19–21] within the gradient-corrected density-functional approximation,[22] employing periodic boundary conditions, norm-conserving pseudopotentials, and using a planewave basis set with energy cutoff of 45 Ry. All electronic-structure parameters and pseudopotentials (except the effective 1 e^- pseudopotential proposed in this work) have been employed in our previous work, see refs [13, 23] for a detailed evaluation of the performance of this approach. For calculations requiring *k*-point sampling of the Brillouin zone, we employ the free-energy functional for finite electronic temperatures in metals[24] with an electronic temperature of 300 K. Structures of the full-coverage monolayer of methylthiolate (MT)/Au(111) were calculated in a $(\sqrt{3}\times\sqrt{3})R30°$ cell, corresponding to three 1×1 Au(111) unit cells. Each cell contains one MT molecule. The cell is periodic in the surface (*xy*) plane and employs a 10 Å vacuum layer between periodic images in the *z*-direction. Structural optimizations were performed with a 6×6 Monkhorst–Pack *k*-point mesh[25] which was found to be sufficient to converge binding energies to within 0.03 eV. All structural optimizations were performed by relaxing the MT molecules and the upper two surface layers of Au atoms to forces of 10^{-3} au or lower. The remaining atoms were frozen in their bulk-lattice positions at the theoretical lattice constant of 4.18 Å. Test calculations on six-layer Au slabs with adsorbed MT molecules, where the upper four surface layers were relaxed, indicate that this approximation has negligible effect on the reported properties.

In constructing an effective pseudopotential, denoted Au*, we considered the following characteristics. First, we aim only at replacing Au atoms located in the fourth layer and below with an effective pseudopotential. Second, it is necessary to minimize the charge transfer across the interface between the 11-valence-e^- Au and Au*, as even a small charge transfer could alter the electronic structure of the surface and of the interface. Third, the bulk lattice constant of the effective pseudopotential should be similar to that of Au so as not to induce unnecessary surface stress. Finally, the pseudopotential must have only a small effect on the structure, energetics and forces of the surface Au atoms and adsorbates such that it may be employed in AIMD simulations without significant loss of accuracy.

The current approach is to employ the scalar relativistic pseudopotential form of ref. [26] for Au*. In this approach the local pseudopotential $V_{loc}(r)$ has the functional form [Eq. (1)]:

$$V_{loc}(r) = (-Z_{ion}/r)\mathrm{erf}(r/\sqrt{2}r_{loc}) + \exp(-1/2(r/r_{loc})^2)\cdot (c_1 + c_2(r/r_{loc})^2 + c_3(r/r_{loc})^4 + c_4(r/r_{loc})^6) \quad (1)$$

where r_{loc}, c_1, c_2, c_3 and c_4 are all variable parameters. Nonlocal projectors are included for p and d electrons with the angular dependent nonlocal potential $V_l(\mathbf{r}, \mathbf{r}')$ given by Equation (2):

$$V_l(\mathbf{r}, \mathbf{r}') = \sum_{i=1}^{3}\sum_{j=1}^{3}\sum_{m=-l}^{+l} Y_{l,m}(\hat{\mathbf{r}})p_i^l(r)h_{ij}^l p_j^l(r')Y_{l,m}^*(\hat{\mathbf{r}}') \quad (2)$$

where $Y_{l,m}^*$ are spherical harmonics, h_{ij}^l are fitting parameters and p^l are projectors [Eq. (3)]:

$$p_i^l(r) = \frac{\sqrt{2}r^{l+2(i-1)}\exp(-r^2/2r_l^2)}{r_l^{l+(4i-1)/2}\sqrt{\Gamma(l+(4i-1)/2)}} \quad (3)$$

where Γ is the gamma function and r_l is also a fitting parameter. In practice, these potentials are fit to atomic data by an iterative fitting scheme[26] and provide excellent transferability.

Given that the potential we wish to generate is only required to model some properties of bulk gold (and is not required to be transferable to molecules or coordination compounds) we may relax some of the stringent criteria normally used in the generation of transferable pseudopotentials. The fitting task is made simple by the crucial observation that the Au/Au* charge transfer, as measured by variations in the electrostatic potential V_{ES} (as defined in the CPMD code, see ref. [21]), is largely controlled by the cutoff distance of the local pseudopotential, r_{loc}. Thus, a series of potentials was generated with different r_{loc} allowing all other parameters to vary to obtain the best fit for atomic Au. The final potential was then chosen which reduced the net amount of charge transfer for a six-layer-thick Au(111) slab where the top and bottom three layers contain Au and Au*, respectively (see next Section for details). The final values of the fitting parameters are: $r_{loc}=0.62$ au, $c_1=62.08$, $c_2=-1.70$, $c_3=c_4=0.0$, $r_1=0.89$ au, $h_{11}^1=-6.32$, $h_{12}^1=0.48$, $h_{13}^1=2.69$, $h_{22}^1=-3.58$, $h_{23}^1=0.49$, $h_{33}^1=-0.79$, $r_2=0.52$ au, $h_{11}^2=66.54$, $h_{12}^2=32.64$, $h_{13}^2=19.45$, $h_{22}^2=77.16$, $h_{23}^2=0.15$, $h_{33}^2=-0.21$.[27]

Results and Discussion

The *z* projection of V_{ES} is shown in Figure 1 for the six-layer slab with three layers of Au* and three layers of Au, as compared with that obtained for a slab where all six layers are Au. The value of V_{ES} between the two models is essentially identical for the upper three atomic layers as a result of the minimal charge transfer. Moreover, there is only a very small dipole

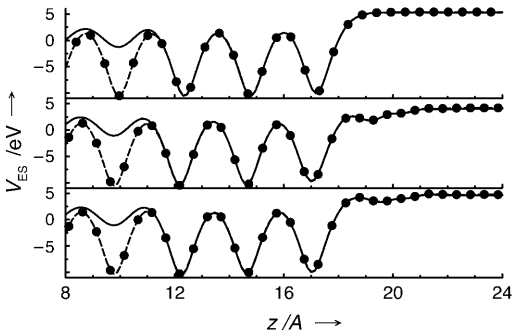

Figure 1. The upper panel in the graph shows the *z* projection of V_{ES} for a clean Au(111) surface as obtained for the calculation where all layers are modeled by an 11 e^- potential (-----, ●) and where the bottom three layers include the effective 1 e^- potential (——). The middle and lower panels show these same functions for MT in the bridge and on-top sites, respectively. The dipole layer resulting from the periodic boundary conditions in the vacuum region has been subtracted in the latter two calculations. The upper layer of Au atoms of the surface slab is at $z=16.5$ Å, whereas the atoms in the MT are located at $z>18.5$ Å.

layer in the vacuum region of the mixed Au/Au* system, which also indicates minimal charge transfer. In Figure 1 $E_{Fermi}=0$, thus providing the work function $\Phi=V_{ES}$ in the vacuum region. For both models $\Phi=5.3$ eV (compared with the experimental value, 5.3 eV[28]), which further demonstrates that the effective pseudopotential does not perturb the interfacial electronic structure to a high degree of accuracy. We also tested the performance of Au* in describing the mechanical properties of bulk gold. The crystal-lattice parameter obtained with Au*, $a=4.12$ Å compares well with $a=4.18$ Å for Au ($a=4.03$ Å experimentally); however, the bulk modulus $B=350$ kbar for Au* is far lower than $B=1550$ kbar for Au ($B=1720$ kbar experimentally). This demonstrates that Au* is not fully suitable to describe the mechanical properties of bulk gold. However, the small lattice mismatch indicates that surface stress is minimal. In fact, we find that the optimized positions of the upper two Au layers differ by 0.01 Å at most in the two slabs, with a maximal difference in force of 10^{-3} au for selected configurations.

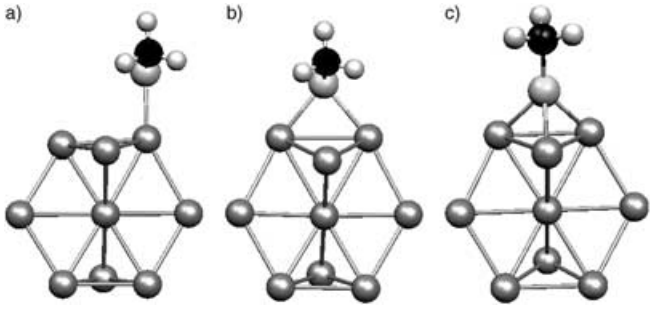

Figure 2. The optimized structure of MT adsorbed on Au(111) at the hcp hollow (a), bridge (b) and on-top (c) sites.

As a more stringent test we examine the transferability of the pseudopotential by considering the case where MT is bound to Au(111) at the hexagonal close-packed (hcp) hollow, bridge and on-top sites, see Figure 2. Specifically, these sites are chosen as they represent three-, two- and one-fold coordination of the thiolate S atom by Au. The bridge site corresponds to the most common theoretical structure[9–11] and the on-top site to the recently advanced experimental one based on X-ray standing waves[14] and photoelectron diffraction.[15] Detailed structural parameters and energetics are presented in Table 1. In agreement with previous findings,[9] comparison between the four- and six-layer all-Au slabs indicate that the structural and energetic quantities under consideration are well converged with respect to slab thickness. This is not true for three-layer slabs which can show significant deviations from calculations with thicker slabs: see Tables I and V of ref. [9]; for example, in a three-layer all-Au calculation the bridge site is found to be 0.22 and 0.20 eV lower in energy than the hcp and on-top sites, respectively, while the converged values, obtained with a six-layer all-Au slab, are 0.47 and 0.35 eV. Hence, the insufficient slab thickness provides a flatter potential-energy landscape, which would severely alter the relative population of the various sites observed in an AIMD simulation. Our Au/Au* mixed slab gives 0.44 and 0.38 eV for these same quantities, in much better agreement with the converged value. Since in both cases the number of variables free to relax in the geometry optimization is the same, this is clearly an electronic effect and not a mechanical one. Similar findings occur for MT binding energies, $E_{binding}$, relative to a clean Au(111) surface and MT gas-phase radical. As shown in Table 1, the effective pseudopotential significantly improves the binding energy of the bridge site, relative to the three-layer slab. There is also substantial agreement between optimized geometries, with Au–S and C–S bonds differing by at most 0.01 Å. However, as this is true even for the three- and four-layer slabs, it may only be concluded that Au* does not alter these quantities.

A very sensitive measure of charge transfer and interfacial electrostatics is given by the work function. Unlike the binding energies, this quantity is well represented by the three- and four-layer slabs, within the accuracy of our calculation. However, this situation could be severely altered if there is charge transfer at the interface between Au and Au*. This is not the case, however, and our values are $\Phi=4.7$, 4.1 and 3.5 eV for the on-top, bridge and hcp sites, respectively, with the all-Au slab, and $\Phi=4.6$, 4.0 and 3.4 eV with the mixed slab. Hence, the effective pseudopotential is able to distinguish semiqualitatively the variations in the interface electrostatics caused by thiolate adsorption, including the subtle differences between coordination sites.

Table 1. Structural parameters, binding energetics ($E_{binding}$), and work function (Φ) for MT on Au(111) for metal-slab models with a three-, a four-, and a six-layer slab of all-Au or a six-layer slab of mixed Au/Au*. The one- and eight-molecule models correspond to the $(\sqrt{3}\times\sqrt{3})R30°$ cell and the $c(3\times4\sqrt{3})$ supercell, respectively.

Binding Site	Molecules	Slab	d_{Au_S} [Å]	d_{S_C} [Å]	$E_{binding}$ [eV]	Φ [eV]
on-top	1	3-Au	2.37	1.82	1.57	4.6
on-top	1	4-Au	2.37	1.82	1.60	4.6
on-top	1	6-Au	2.36	1.82	1.61	4.7
on-top	1	6-Au/Au*	2.37	1.82	1.55	4.6
bridge	1	3-Au	2.47	1.84	1.77	4.0
bridge	1	4-Au	2.46	1.84	1.90	4.1
bridge	1	6-Au	2.45	1.84	1.96	4.1
bridge	1	6-Au/Au*	2.45	1.84	1.93	4.0
hcp	1	3-Au	2.46	1.86	1.55	3.4
hcp	1	4-Au	2.48	1.86	1.47	3.4
hcp	1	6-Au	2.48	1.85	1.49	3.5
hcp	1	6-Au/Au*	2.49	1.85	1.49	3.4
bridge	8	6-Au	2.46	1.84	1.95	4.1
bridge	8	6-Au/Au*	2.47	1.83	2.09	3.9

To illustrate the use of this pseudopotential in an AIMD simulation we have performed a 5 ps molecular dynamics simulation at $T=100$ K of an eight-molecule six-atomic-layer-thick slab in a $c(3\times4\sqrt{3})$ supercell of the $(\sqrt{3}\times\sqrt{3})R30°$ structure. The upper three Au layers are modeled by our $11\,e^-$ potential and the lower three layers by Au* with the atomic coordinates of the bottom four layers frozen to their bulk lattice position. The simulation has 968 valence electrons which is a reduction of 43% relative to a calculation containing all Au-$11\,e^-$ atoms explicitly and 17% relative to a four-layer-slab calculation. In terms of the computational effort this corresponds to a reduction in the duration of a MD time step, using the CPMD code, by a factor of about $^1/_3$ and $^2/_3$ relative to a six- and four-layer-thick slab, respectively, see ref. [21] for details on scaling of the computational cost with system size. For these calculations we employ only the Γ point for BZ sampling and perform the AIMD simulations in the Car–Parrinello (CP) approximation[19]

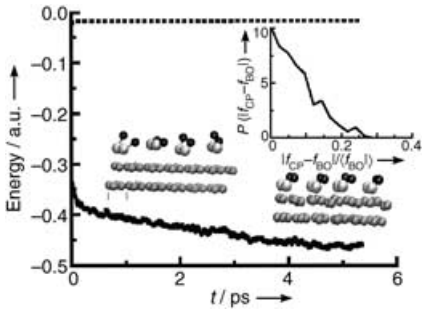

Figure 3. The Kohn–Sham (——) and total (-----) energies during a 5 ps CP simulation at constant $T=100$ K. The structures shown in the graph represent Au, S and C positions of the initial (left) and final (right) configuration. The inset shows the probability distribution, P, of the error in the forces, f, between the CP and BO MD wavefunctions, $f_{CP}-f_{BO}$, relative to the average BO value, as compiled by sampling well-separated configurations.

with a time step of 2 au and massive thermostating on the electrons and nuclei.[17,29] This approximation allows us to maintain a well-conserved total energy throughout the dynamics, see Figure 3. Following our previous work,[30] as a check on the CP approximation we examine the relative forces obtained for a few well-separated configurations during the CPMD run relative to the forces obtained from the Born–Oppenheimer ground-state wavefunction. The forces obtained from the CP only deviate from those from the Born–Oppenheimer approximation by about 10% of an average value of $\approx10^{-2}$ au with an approximate Gaussian distribution; see inset in Figure 3.

As starting configuration we employ a planar Au(111) surface and eight thiolate molecules oriented randomly (see left structure in Figure 3) with the S atoms about 3.0–3.5 Å above the face-centered cubic (fcc) hollow site. The structure is then allowed to slowly relax over a time scale of about 5 ps with a constant temperature of $T=100$ K. The resulting structure, which displays a rough gold surface and all eight thiolate molecules at the bridge site, is then annealed to 0 K: see Table 1 for structural parameters and Figure 3 for graphical view. The structure compares rather well with the bridge configuration as obtained from our $(\sqrt{3}\times\sqrt{3})R30°$ k-point-converged calculations, but exhibits a 0.16-eV-larger binding energy and an average deviation of the top-most Au of 0.15 Å from the mean surface plane as opposed to 0.11 Å from the small-cell calculation. To test that our effective potential has found a realistic minimum for this cell, and to determine if the deviations from the single-molecule cell are a result of k-point sampling or results from the potential, we replaced the bottom three atomic layers with $11\,e^-$ Au atoms and re-optimized the structure via a rapid quenching of the ions and electrons. The resulting structure is almost identical, with maximum atomic displacement of 0.02 Å, to that obtained with the effective pseudopotential but does exhibit a binding energy and Φ closer to that of the k-point-converged one-molecule cell (see Table 1). However, the relative error of 0.1–0.2 eV in both binding energy and Φ observed in the k-point calculations is also found here, supporting the idea of transferability of the potential. Hence, the combination of approximations, including the supercell, CP formalism and effective pseudopotential are able to generate reasonable representations of the potential-energy landscape for these systems.

Conclusions

We have generated an effective $1\,e^-$ pseudopotential for Au which allows us to mimic the structural, energetic and electrostatic properties of a six-atom-thick Au slab. This potential radically reduces the computational task associated with metal-slab calculations and enables us to perform AIMD simulations of Au SAMs with reasonable computational demand.

These results underscore the importance of the bridge configuration as the energetically preferred binding site for MT on Au(111), in agreement with previous studies,[9–11,13] but do not provide any further insight as to why measurements, such as X-ray standing-wave spectroscopy, are better explained by an on-top model.[14] One possibility is a Au-surface reconstruction, similar to that suggested by Molina and Hammer,[11] which may occur on longer time scales than those accessed here. This would make the unreconstructed MT/Au(111) species observed here only a local minimum on the potential-energy landscape with an as yet undetermined global minimum for a reconstructed Au surface. Future work will focus on employing this potential in longer AIMD simulations at higher temperatures in order to investigate this hypothesis as well as explore the role of thermal fluctuations on the structure and properties of these materials.

Acknowledgments

The Authors are grateful to the Italian Ministry for Education, Universities and Research for a COFIN grant, as well as SISSA, ICTP and INFM for computer time. R.R.'s position in SISSA was sponsored by a MIUR contract. We thank L. Casalis, A. Morgante, G. Scoles, V. De Renzi and M. Konôpka for insightful discussions.

Keywords: ab initio calculations · density functional calculations · gold · self-assembly · thiolates

[1] G. Yang, G.-Y. Liu, *J. Phys. Chem. B* **2003**, *107*, 8746.
[2] a) J. Reichert, R. Ochs, D. Beckmann, H. B. Weber, M. Mayor, H. v. Löhneysen, *Phys. Rev. Lett.* **2002**, *88*, 176804; b) C. Zhou, M. R. Deshpande, M. A. Reed, J. M. Tour, *Appl. Phys. Lett.* **1997**, *71*, 611.
[3] S. J. Metallo, R. S. Kane, R. E. Holmlin, G. M. Whitesides, *J. Am. Chem. Soc.* **2003**, *125*, 4534.
[4] H. Sellers, A. Ulman, Y. Shnidman, J. E. Eilers *J. Am. Chem. Soc.* **1993**, *115*, 9389.
[5] K. M. Beardmore, J. D. Kress, N. Gronbeck–Jenson, A. R. Bishop, *Chem. Phys. Letts.* **1998** *40*, 286.
[6] H. Gronbeck, A. Curioni, W. Andreoni, *J. Am. Chem. Soc.* **2000**, *122*, 3839.
[7] D. Fischer, A. Curioni, W. Andreoni, *Langmuir* **2003**, *19*, 3567.
[8] a) Y. Yourdshahyan, H. K. Zhang, A. M. Rappe, *Phys. Rev. B* **2001**, *63*, 081405(R); b) Y. Yourdshahyan, A. M. Rappe, *J. Chem. Phys.* **2002**, *117*, 825.
[9] T. Hayashi, Y. Morikawa, H. Nozoye, *J. Chem. Phys.* **2001**, *114*, 7615.
[10] M. C. Vargas, P. Giannozzi, A. Selloni, G. Scoles, *J. Phys. Chem.* **2001**, *105*, 9509.
[11] a) J. Gottschalck, B. Hammer, *J Chem. Phys* **2002** *116*, 784; b) L. M. Molina, B. Hammer *Chem. Phys. Lett.* **2002** *360*, 264.
[12] S. Piccinin, A. Selloni, S. Scandolo, R. Car, G. Scoles, *J. Chem. Phys.* **2003**, *119*, 6729.
[13] M. Konôpka, R. Rousseau, I. Štich, D. Marx, *J. Am. Chem. Soc.* **2004**, *126*, 12103.
[14] M. G. Roper, M. P. Skegg, C. J. Fisher, J. J. Lee, V. R. Dhanak, D. P. Woodruff, R. G. Jones, *Chem. Phys. Lett.* **2004**, *389*, 87.
[15] H. Kondoh, M. Iwasaki, T. Shimada, K. Amemiya, T. Yokoyama, T. Ohta, M. Shimomura, S. Kono, *Phys. Rev. Lett.* **2003**, *90*, 066102.
[16] V. De Renzi, R. Di Felice, D. Marchetto, R. Biagi, U. del Pennino, A. Selloni, *J. Phys. Chem. B* **2004**, *108*, 16.
[17] D. Krüger, H. Fuchs, R. Rousseau, D. Marx, M. Parrinello, *Phys. Rev. Lett.* **2002**, *89*, 186 402.
[18] U. Landman, W. D. Luedtke, N. A. Burnham, R. J. Colton, *Science* **1990**, *248*, 454.
[19] R. Car, M. Parrinello, *Phys. Rev. Lett.* **1985**, *55*, 2471.
[20] CPMD V3.9, Copyright IBM Corp 1990–2001, Copyright MPI für Festkoerperforschung Stuttgart, **1997–2001**.
[21] D. Marx, J. Hutter in *Modern Methods and Algorithms of Quantum Chemistry* (Ed.: J. Grotendorst), NIC, Forschungszentrum Jüich, **2000**, p. 301. For download see http://www.fz-juelich.de/nic-series/Volume1/marx.pdf.
[22] J. P. Perdew, K. Burke, M. Ernzerhof, *Phys. Rev. Lett.* **1996**, *77*, 3865.
[23] D. Krüger, H. Fuchs, R. Rousseau, D. Marx, M. Parrinello, *J. Chem. Phys.* **2001**, *115*, 4776.
[24] A. Alavi, J. Kohanoff, M. Parrinello, D. Frenkel, *Phys. Rev. Lett.* **1994**, *73*, 2599.
[25] H. J. Monkhorst, J. D. Pack, *Phys. Rev. B* **1976**, *13*, 5188.
[26] C. Hartwigsen, S. Goedecker, J. Hutter. *Phys. Rev. B* **1998**, *58*, 3641.
[27] The potential in CPMD format is available from the authors by request.
[28] D. R. Lide, *CRC Handbook of Physics and Chemistry*, 83rd edition, CRC Press, New York, **2003**.
[29] P. E. Blöchl, M. Parrinello, *Phys. Rev. B* **1992**, *45*, 9413.
[30] P. Tangney, S. Scandolo, *J. Chem. Phys.* **2002**, *116*, 14.

Received: December 12, 2004

